ACS Catalysis

Research Article

pubs.acs.org/acscatalysis

Combination of Enzyme and Ru−B Amorphous Alloy Encapsulated in Yolk-Shell Silica for One-Pot Dextrin Conversion to Sorbitol

Liang Xu, Wei Wei, Hexing Li, and Hui Li*

The Education Ministry Key Lab of Resource Chemistry and Shanghai Key Laboratory of Rare Earth Functional Materials, Shanghai Normal University, Shanghai 200234, P. R. China

Supporting Information

ABSTRACT: In this paper, one-pot dextrin hydrolysis to glucose and the subsequent glucose hydrogenation to sorbitol is successfully conducted by using amyloglucosidase and Ru−B amorphous alloy highly dispersed onto the ordered mesoporous silica encapsulated by a porous silica shell. The porous outer silica shell prevents the larger amyloglucosidase and colloidal hydrolysis substances from contacting Ru−B, which avoids the poisoning effect on each other. Meanwhile, the small glucose can directly access the Ru−B cores through the pores within the silica shells, and the produced sorbitol can readily exit through these pores. Thus, both the amyloglucosidase-aided dextrin hydrolysis and the Ru−B-catalyzed glucose hydrogenation proceed efficiently in bulk solution and inside the chamber, respectively, leading to high sorbitol yield and strong durability. The catalyst design concept used in such a yolk-shell structured configuration opens a new avenue for the development of a highly efficient catalyst system for one-pot cascade reactions containing incompatible parameters.

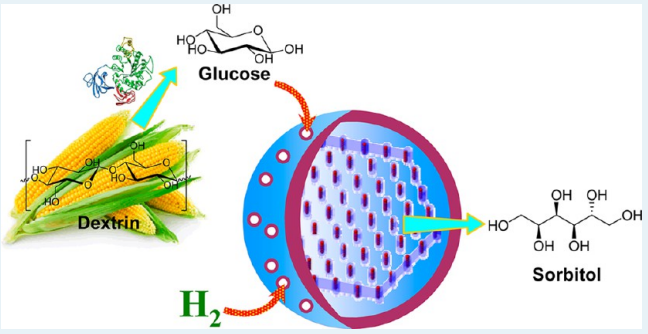

KEYWORDS: *biomass conversion, sorbitol, amorphous alloy catalyst, hydrolysis, hydrogenation*

INTRODUCTION

As one of the top 12 biobased building blocks listed by the U.S. Department of Energy,[1] sorbitol is a valuable platform molecule that can be facilely transformed into fuels or chemicals.[2,3] Nowadays, practically all of the sorbitol is produced *via* hydrogenation of glucose,[4−11] obtained mostly by hydrolysis of starches,[12−14] which represents a hot-topic for the production of highly valuable chemicals from starches. Up to now, various catalysts including enzymes, Brönsted and Lewis acids, etc. have been developed for hydrolysis of starches.[12−14] Meanwhile, a great number of metal and organometal catalysts have also been designed for glucose hydrogenation.[4−11] Apparently, one-pot production of sorbitol from starch displays advantages in simplifying operation and lowering the cost mainly linked to separation and refining procedures.[15−17] One-pot hydrolysis-hydrogenation of inulin can be conducted to form mannitol and sorbitol with a Ru−P(m-$C_6H_4SO_3Na$)$_3$ catalyst.[18] But this homogeneous catalysis presents a number of drawbacks, particularly the catalyst reusability. A one-pot process for the production of sorbitol from glucan-type polysaccharides (especially starch) where hydrolysis and hydrogenation reactions were combined has been developed using Ru supported on acidic zeolite as a bifunctional catalyst;[19] however, this process includes harsh reaction conditions (453 K). Additionally, one critical issue associated with acid-catalyzed hydrolysis of polysaccharides is the formation of undesirably colored and flavored breakdown products.[13] The formation of byproducts makes a purification of product necessary and eventually increases the overall cost.

Enzymes have been widely used in the hydrolysis of starches owing to their high activities even under moderate conditions (328−348 K).[20] The amyloglucosidase represents a typical enzyme most frequently employed in starch hydrolysis to glucose. However, our preliminary studies revealed that the amyloglucosidase is easily poisoned when it is in direct contact with Ru-based metal catalysts. Meanwhile, the presence of amyloglucosidase and the colloidal substances resulted from dextrin hydrolysis also rapidly deactivated the Ru-based metal catalysts in the subsequent glucose hydrogenation to sorbitol. Herein, we report for the first time a novel catalyst system containing free amyloglucosidase and Ru−B amorphous catalyst deposited onto the ordered mesoporous silica ($mSiO_2$) as a core encapsulated by a porous SiO_2 shell (Ru−B/$mSiO_2$@air@SiO_2), which was used in one-pot dextrin conversion to sorbitol comprised of the amyloglucosidase-catalyzed dextrin hydrolysis to glucose and the Ru−B-catalyzed glucose hydrogenation to sorbitol. By controlling the pore size, the outer SiO_2 shell allowed small glucose molecules to diffuse inside the chamber for subsequent hydrogenation on the Ru−B/$mSiO_2$ amorphous catalyst. The large-sized amyloglucosidase molecules and colloidal substances resulted from dextrin

Received: September 24, 2013
Revised: November 5, 2013
Published: December 11, 2013

Scheme 1. Synthesis of Yolk-Shell Ru−B/mSiO$_2$@air@SiO$_2$

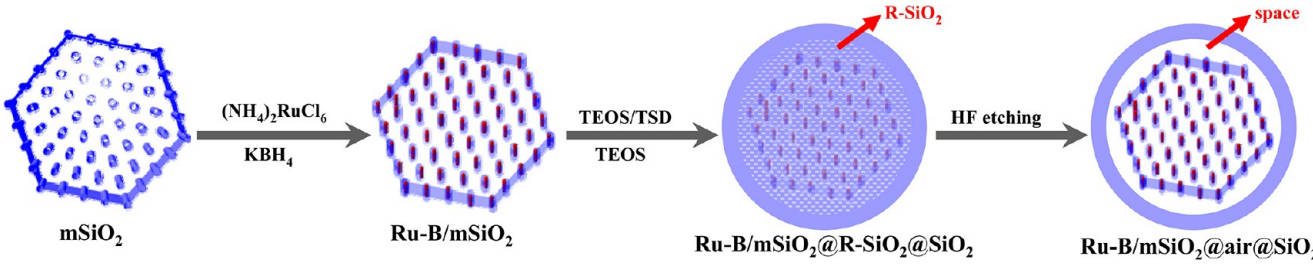

hydrolysis could not pass through the outer SiO_2 shell to contact Ru−B, which could effectively prevent the deactivation of either the amyloglucosidase or the Ru−B amorphous catalyst. Meanwhile, the yolk-shell structure also promoted the glucose hydrogenation efficiency owing to the microreactor effect.[21,22] Moreover, the Ru−B/mSiO$_2$@air@SiO$_2$ could be easily recycled and exhibited strong durability in repetitive uses.

EXPERIMENTAL PROCEDURES

Catalyst Preparation. Tetraethoxysilane (TEOS), *N*-[3-(trimethoxysilyl)propyl]ethylenediamine (TSD), P123 ($EO_{20}PO_{70}EO_{20}$), hydrofluoric acid (HF), $(NH_4)_2RuCl_6$, KBH_4, amyloglucosidase (glucoamylase; exo-1,4-α-glucosidase; EC 3.2.1.3 from *Aspergillus niger*; 100 000 units/ml), and dextrin were purchased from Aladdin Industrial Co., Ltd. (Shanghai, China) and were used without any other treatments. The synthesis of yolk-shell Ru−B/mSiO$_2$@air@SiO$_2$ is in three steps (Scheme 1). (1) Uniform dispersing of Ru−B amorphous alloys within the porous channels of ordered mesoporous silica (Ru−B/mSiO$_2$) was achieved by ultrasound-assisted incipient wetness infiltration of $(NH_4)_2RuCl_6$ onto mSiO$_2$, followed by reduction with BH_4^-.[23] First, mesoporous silica was synthesized following the method described by Chen et al..[24] Briefly, 1.0 g of P123 was dissolved in 45 mL of 2.0 M HCl aqueous solution containing 0.161 g of $ZrOCl_2{\cdot}8H_2O$. The mixture was stirred at 308 K for 3.0 h, followed by adding 10 mmol of TEOS. After being stirred at 308 K for 1 day and aged at 373 K for another day under static conditions, the solid product was thoroughly washed with deionized water, followed by drying at 373 K. The as-prepared sample was heated at 773 K for 3.0 h to obtain the calcined sample mSiO$_2$. Then, the supported Ru−B catalysts were prepared as follows:[23] 1.0 g of mSiO$_2$ was impregnated with a certain mount of NH_4RuCl_6 aqueous solution (0.02 g/mL), which was sonicated for 2 h with an ultrasonic batch (60 W). After being calcined at 393 K for 0.5 h, 10 mL of KBH_4 aqueous solution (0.027 g/mL) was added dropwise at 273 K and was stirred continuously until no bubbles were released. The solid was washed free from Cl^- and K^+ ions with deionized water until a pH of ∼7 was achieved. (2) The Ru−B/mSiO$_2$ particles were encapsulated by co-condensation of TEOS and TSD, generating a sandwich structured Ru−B/mSiO$_2$@R-SiO$_2$@SiO$_2$, where R-SiO$_2$ refers to an organofunctionalized SiO$_2$ layer between the Ru−B/mSiO$_2$ core and the pure SiO$_2$ outer shell. Sandwich structured Ru−B/mSiO$_2$@R-SiO$_2$@SiO$_2$ was fabricated according to the modified Stöber method reported by Chen et al.[25] In a typical run of synthesis, 1.0 g of Ru−B/mSiO$_2$ was added in a solution comprised of 60 mL of 28% aqueous ammonia and 180 mL of ethanol, which was sonicated for 10 min with an ultrasonic bath (60 W). Then, the mixture was stirred for 10 min at 308 K. Next, 8.0 mL of TEOS and 8.0 mL of ethanol containing 0.3 mL of TSD were added dropwise into the previous mixture synchronously and stirred for 30 min, to form the middle layer of organic silica framework. Afterward, 8.0 mL of TEOS was added and stirred for 6.0 h, to form the outer layer of the silica shell. After being thoroughly washed with ethanol and deionized water, the sandwich structured Ru−B/mSiO$_2$@R-SiO$_2$@SiO$_2$ was dispersed in 60 mL of deionized water. (3) The as-prepared sandwich structured Ru−B/mSiO$_2$@R-SiO$_2$@SiO$_2$ was selectively etched with a certain amount of HF to remove R-SiO$_2$, leading to yolk-shell Ru−B/mSiO$_2$@air@SiO$_2$ configurations. In a typical run of synthesis, 1.0 mL of 40% HF was added dropwise into Ru−B/mSiO$_2$@SiO$_2$@SiO$_2$ suspension and stirred for 5 min. Finally, yolk-shell structured Ru−B/mSiO$_2$@air@SiO$_2$ was obtained by centrifugation and washing with plenty of water.

Catalyst Characterization. The bulk composition and Ru loading were analyzed by means of inductively coupled plasma optical emission spectrometry (ICP-OES; Varian VISTA-MPX). The amorphous structure was determined by both X-ray diffraction (XRD; Rigaku D/Max-RB with Cu Kα radiation) and selective-area electronic diffraction (SAED; JEOL JEM2100). The crystallization process was followed by differential scanning calorimetry (DSC; Shimadzu DSC-60) under an N_2 atmosphere at the heating rate of 10 K/min. The catalyst shapes and morphologies were observed by both field emission scanning electron microscopy (FESEM; HITACHI S-4800) and transmission electron microscopy (TEM; JEOL JEM2100). X-ray photoelectron spectroscopy (XPS) measurements were performed on a ULVAC-PHI PHI5000 VersaProbe system using Al Kα radiation, during which all samples were dried and pretreated *in situ* in a pure Ar atmosphere to avoid oxidation. All the BE values were calibrated by using C 1s = 284.6 eV as a reference. N_2 adsorption−desorption isotherms were obtained at 77 K using a Quantachrome NOVA 4000e apparatus. By N_2 adsorption, the Brunauer−Emmett−Teller (BET) surface area (S_{BET}) was calculated by using the multiple-point BET method in the relative pressure range of P/P_0 = 0.05−0.2. The pore volume and pore size distribution curve were obtained by the Barrett−Joyner−Halenda model. The active surface area (S_{Ru}) was measured by hydrogen chemisorption at room temperature, which was performed on a Micromeritics AutoChem II 2920 instrument using a dynamic pulse method. The sample was purged under an argon flow (purity of 99.997%, treated with an Alltech Oxy-Trap column) at 523 K for 2 h. The pretreated sample was cooled down to room temperature under an argon atmosphere, and hydrogen pulses were injected at 303 K until the calculated areas of consecutive pulses were constant. According to the hydrogenation chemisorption, S_{Ru} of the as-prepared catalyst was calculated assuming Ru/H = 1 and a Ru surface density of 1.64 × 10^{19} atoms m^{-2}.[26] Every sample was measured three times.

dx.doi.org/10.1021/cs400853u | ACS Catal. 2014, 4, 251−258

The reproducibility of the results was checked by repeating the measurements three times on the same catalyst and was found to be within acceptable limits (< ±2%). Then, hydrogen temperature-programmed desorption (H_2-TPD) curves were obtained on the same instrument in argon flow by raising the temperature at a ramping rate of 10 K/min in which the released H_2 was determined by TCD. Dynamic light scattering (DSL) was obtained from Malvern Zetasizer Nano ZS 90.

Activity Test. In a typical experiment, the one-pot hydrolysis−hydrogenation of dextrin to sorbitol was carried out in a Parr 5521 autoclave containing Ru−B/$mSiO_2$@air@SiO_2 (26 mg Ru), 0.08 mL of amyloglucosidase, 1.0 g of dextrin, 100 mL of water, and 6.0 MPa of H_2 at 348 K. The reaction system was stirred vigorously (800 rpm) to eliminate the diffusion effect. The reaction mixture was sampled at intervals for product analysis on a liquid-phase chromatograph (Agilent 1200) equipped with a carbohydrate column (Shodex, SC1011) and a refractive index detector at 333 K with water as the movable phase at 0.5 mL/min. After cooling to room temperature at the end of the reaction, the yolk-shell structured catalyst was separated by centrifugation and washed with deionized water for further characterizations and applications. In order to determine the catalyst durability, the used Ru−B/$mSiO_2$@air@SiO_2 catalyst was centrifuged and washed thoroughly with distilled water after each run of the reaction. Then, the Ru−B/$mSiO_2$@air@SiO_2 was reused with a fresh charge of dextrin and fresh amyloglucosidase for subsequent recycle runs under the same reaction conditions.

RESULTS AND DISCUSSION

Catalyst Characterization. As shown in Figure 1, the FESEM images reveal that the $mSiO_2$ was present in hexagonal

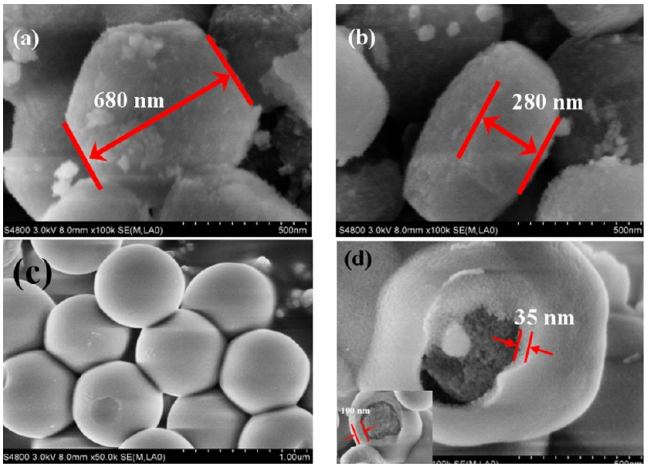

Figure 1. FESEM images of the $mSiO_2$ (a, b) and the Ru−B/$mSiO_2$@air@SiO_2 (c, d). The inset is the FESEM image of Ru−B/$mSiO_2$@R-SiO_2@SiO_2 before HF etching.

platelets of *ca.* 680 nm width and 280 nm thickness. The Ru−B/$mSiO_2$@air@SiO_2 displayed uniform microspheres with an average diameter around 750 nm. The attached FESEM of broken Ru−B/$mSiO_2$@R-SiO_2@SiO_2 clearly demonstrated that the Ru−B/$mSiO_2$ was encapsulated by the SiO_2 shell with an average thickness of around 100 nm. After being etched with HF solution, the SiO_2 shell thickness decreased to about 35 nm, together with the formation of a space between the SiO_2 shell and the Ru−B/$mSiO_2$ core that could be attributed to the removal of the middle R-SiO_2 layer.

Figure 2 shows the TEM images of different samples. As shown in Figure 2a, the $mSiO_2$ displayed hexagonal platelets

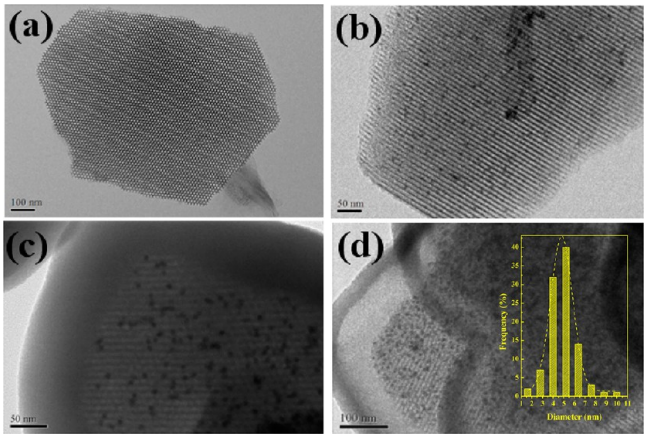

Figure 2. TEM images of (a) $mSiO_2$, (b) Ru−B/$mSiO_2$, (c) Ru−B/$mSiO_2$@R-SiO_2@SiO_2, and (d) Ru−B/$mSiO_2$@air@SiO_2. The inset in d is the corresponding Ru−B size distribution histogram of Ru−B/$mSiO_2$@air@SiO_2.

containing ordered mesoporous channels arrayed along the side of the platelet. The low-angle XRD pattern, N_2 adsorption−desorption isotherm, and pore size distribution curve (Figure S1) further confirmed the ordered 2D-hexagonal (*p6mm*) mesoporous structure centered around 7.0 nm with high S_{BET} of 714 m^2/g. Figure 2b demonstrated that Ru−B/$mSiO_2$ with a Ru loading of 2.60 wt % contained a similar mesoporous structure to the parent $mSiO_2$, and the Ru−B nanoparticles were uniformly dispersed into the pore channels. Figure 2c further revealed that, in the Ru−B/$mSiO_2$@R-SiO_2@SiO_2, the $mSiO_2$ core was completely encapsulated by a silica shell with a thickness around 100 nm without significant damage of either the ordered mesoporous channels or the uniform distribution of Ru−B nanoparticles. From Figure 2d, we could see that, after being etched in HF solution, the silica shell decreased to about 35 nm, together with the formation of a space around 65 nm between the silica shell and the $mSiO_2$ core, obviously due to the removal of the middle R-SiO_2 layer. Again, no significant damage of either the ordered mesoporous structure or the uniform distribution of Ru−B nanoparticles was observed in the Ru−B/$mSiO_2$@air@SiO_2. However, the low-angle XRD patterns (Figure 3) clearly showed an intensity decrease of the diffraction peaks, suggesting that the deposition of Ru−B on the $mSiO_2$ and the subsequent encapsulation of the Ru−B/$mSiO_2$ core caused a decrease in ordering degree of mesoporous structure.

The XPS spectra (Figure 4) revealed that all the Ru species in either the Ru−B/$mSiO_2$ or the Ru−B/$mSiO_2$@air@SiO_2 were present in the metallic state, corresponding to the BE of 279.9 eV in Ru $3d_{5/2}$ while the B species were present in the elemental state and B_2O_3 with a BE of 188.1 and 193.2 eV in B 1s level. The BE of elemental B was shifted positively by 1.0 eV in comparison with the BE of pure B,[27] suggesting the formation of a Ru−B alloy in which partial electrons transferred from B to Ru.[9,23] No significant BE shift of metal Ru was observed, possibly due to its relatively big atomic size comparing the B atom.

dx.doi.org/10.1021/cs400853u | *ACS Catal.* 2014, 4, 251−258

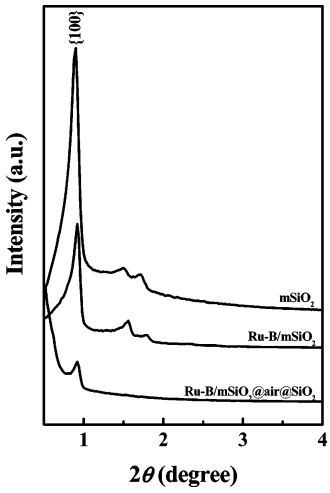

Figure 3. Low-angle XRD patterns of $mSiO_2$, Ru−B/$mSiO_2$, and Ru−B/$mSiO_2$@air@SiO_2.

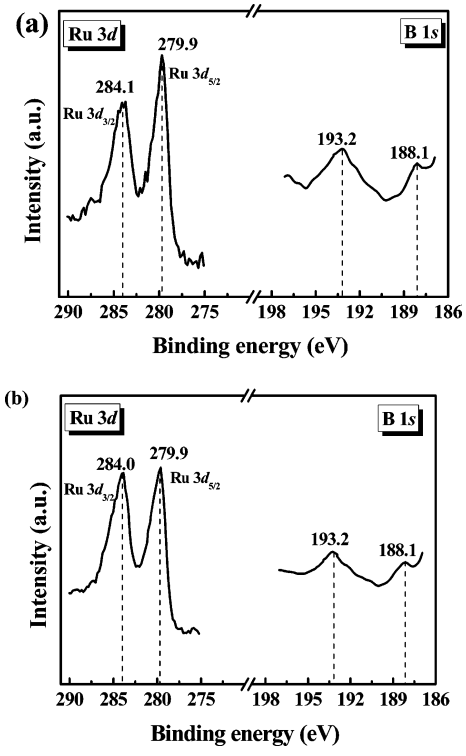

Figure 4. XPS spectra of (a) Ru−B/$mSiO_2$ and (b) Ru−B/$mSiO_2$@air@SiO_2.

The wide-angle XRD patterns (Figure 5) demonstrated that the Ru−B alloy in either the Ru−B/$mSiO_2$ or the Ru−B/$mSiO_2$@air@SiO_2 was present in a typical amorphous alloy structure state, corresponding to a broad peak around 2θ = 45°,[9,23] which was further confirmed by the consecutive diffraction halos in the attached SAED pictures.[28]

From the DSC curves (Figure 6), we could see that the Ru−B/$mSiO_2$@air@SiO_2 exhibited an exothermic peak around 615 K, which was 86 K higher than the Ru−B/$mSiO_2$, suggesting the enhanced thermal stability of Ru−B amorphous alloy against crystallization owing to the encapsulation of Ru−B/$mSiO_2$ by the SiO_2 shell which prevents the Ru−B/$mSiO_2$ from direct heating.

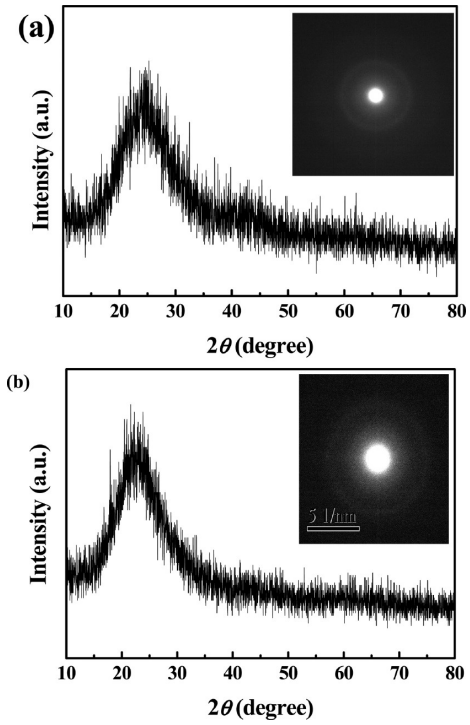

Figure 5. Wide-angle XRD patterns of (a) Ru−B/$mSiO_2$ and (b) Ru−B/$mSiO_2$@air@SiO_2. Insets are the SAED images.

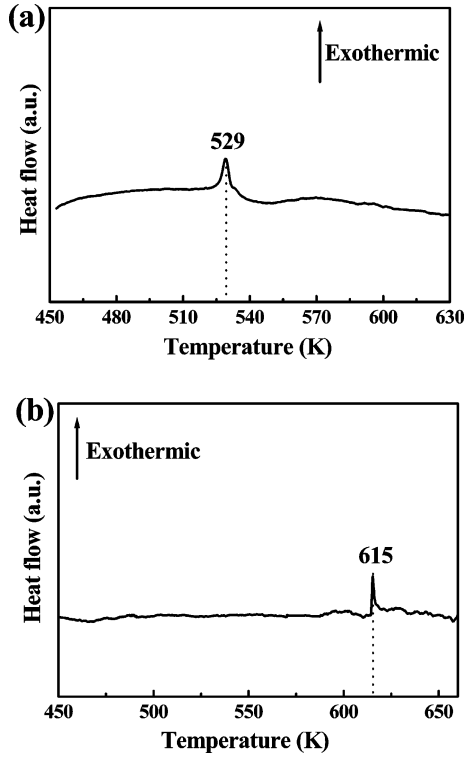

Figure 6. DSC curves of (a) Ru−B/$mSiO_2$ and (b) Ru−B/$mSiO_2$@air@SiO_2.

Catalytic Performances. One-pot conversion of dextrin to sorbitol was used to evaluate the performances of the catalyst system comprising free amyloglucosidase and Ru−B/$mSiO_2$@air@SiO_2 (see Scheme 2). Preliminary studies revealed that both Ru−B/$mSiO_2$ and Ru−B/$mSiO_2$@air@SiO_2 amorphous

dx.doi.org/10.1021/cs400853u | ACS Catal. 2014, 4, 251−258

Scheme 2. One-Pot Production of Sorbitol through Hydrolysis-Hydrogenation of Dextrin by the Merger of Enzymatic and Metal Catalysis

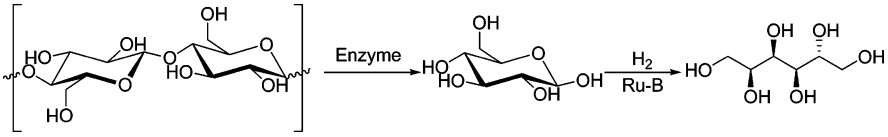

alloy catalysts displayed nearly 100% selectivity toward sorbitol during glucose hydrogenation in aqueous solution. With the increase of the Ru loading, the activity of the Ru−B/mSiO$_2$ in glucose hydrogenation first increased and then decreased (Figure S2a), which can be attributed to the effect of Ru loading on the active surface area (Figure S2b). A similar phenomenon was also found in our recent studies on the supported Pd catalysts.[29] The maximum activity was obtained at a Ru loading of 2.60 wt % with an atom composition of $Ru_{74}B_{26}$, corresponding to the highest S_{Ru}. The 2.60 wt % Ru−B/mSiO$_2$ was therefore selected for the following studies.

Figure 7 shows the dextrin hydrolysis and the glucose hydrogenation in different catalyst systems. Obviously, the

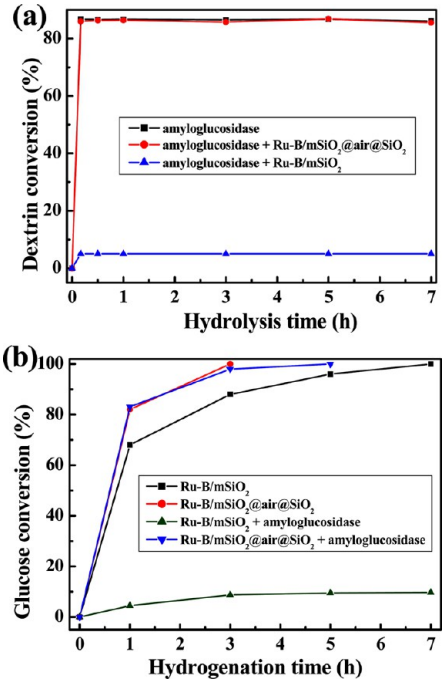

Figure 7. (a) Dextrin hydrolysis and (b) glucose hydrogenation in different catalyst systems. Reaction conditions: dextrin (1.0 g) or glucose (1.0 g/100 mL), amyloglucosidase (0.080 mL), a catalyst containing 26 mg Ru, water (100 mL), T = 348 K, P_{H2} = 6.0 MPa, stirring rate = 800 rpm.

presence of Ru−B/mSiO$_2$ could almost completely suppress the activity of amyloglucosidase in dextrin hydrolysis. However, the presence of Ru−B/mSiO$_2$@air@SiO$_2$ displayed no significant influence on the activity of amyloglucosidase. Concerning the glucose hydrogenation, the presence of amyloglucosidase greatly inhibited the activity of Ru−B/mSiO$_2$ but displayed no significant influence on the activity of Ru−B/mSiO$_2$@air@SiO$_2$. These results demonstrated that the amyloglucosidase and Ru−B/mSiO$_2$ may poison each other in dextrin hydrolysis and glucose hydrogenation, respectively, if they are in direct contact with each other. The outer SiO$_2$ shell in Ru−B/mSiO$_2$@air@SiO$_2$ played a key role in avoiding the poisoning effect by inhibiting the direct contact between amyloglucosidase and Ru−B/mSiO$_2$. We also prepared pure SiO$_2$, followed by etching with the same amount of HF as that used in synthesis of Ru−B/mSiO$_2$@air@SiO$_2$. The N_2 adsorption−desorption isotherm demonstrated that the SiO$_2$ after being etched in HF solution contained multiple pore channels with a broad pore size distribution from 3 to 30 nm (Figure S3). Taking into account that the amyloglucosidase is about 100−1000 nm (see Figure S4a), the porous SiO$_2$ outer shell in the Ru−B/mSiO$_2$@air@SiO$_2$ could efficiently prevent the diffusion of amyloglucosidase into the chamber to contact the Ru−B/mSiO$_2$ core and thus avoids the poisoning effects. Additionally, the dextrin molecule and other colloidal substances resulted from the dextrin hydrolysis are bigger, more than 1000 nm (see Figure S4b). Therefore, they also could not pass through the porous SiO$_2$ outer shell. This ensured that the dextrin hydrolysis occurred absolutely outside the Ru−B/mSiO$_2$@air@SiO$_2$ microspheres and therefore protects the Ru−B/mSiO$_2$ from poisoning by dextrin and other colloidal substances resulted from the dextrin hydrolysis. However, the glucose could easily diffuse through the porous SiO$_2$ outer shell owing to its small molecular size (∼1 nm), followed by adsorption and hydrogenation on the Ru−B/mSiO$_2$ core. The product sorbitol could also easily diffuse into the bulk solution by passing through the outer SiO$_2$ shell owing to its small molecular size. Thus, in the present system, the amyloglucosidase and Ru−B/mSiO$_2$@air@SiO$_2$ could retain their own activities in dextrin hydrolysis and glucose hydrogenation, respectively. Concerning the glucose hydrogenation to sorbitol in the absence of amyloglucosidase, it is interesting to see that the Ru−B/mSiO$_2$@air@SiO$_2$ exhibited slightly higher activity than the Ru−B/mSiO$_2$. Several factors might possibly account for the enhanced activity of the Ru−B/mSiO$_2$@air@SiO$_2$. (1) A much higher amount of the desorbed hydrogen is observed for Ru−B/mSiO$_2$@air@SiO$_2$ than that for Ru−B/mSiO$_2$ during H_2-TPD experiments (Figure 8), indicating a higher concentration of active hydrogen species

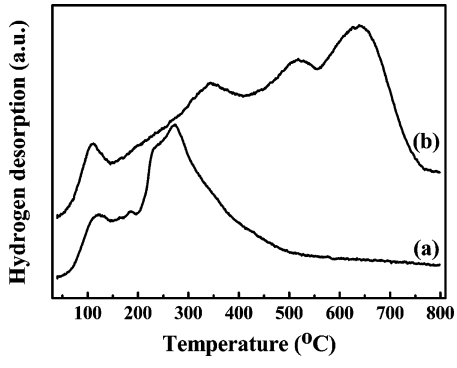

Figure 8. H_2-TPD profiles of (a) Ru−B/mSiO$_2$ and (b) Ru−B/mSiO$_2$@air@SiO$_2$. The signal is normalized based on unit mass Ru.

dx.doi.org/10.1021/cs400853u | ACS Catal. 2014, 4, 251−258

inside the yolk-shell structured nanoreactor, which favors the hydrogenation reaction. (2) The yolk-shell configuration of Ru−B/mSiO$_2$@air@SiO$_2$ might enrich the glucose molecules in the chamber owing to the microreactor effect. (3) The yolk-shell configuration of Ru−B/mSiO$_2$@air@SiO$_2$ might effectively increase the collision frequency between reactants and Ru active sites inside the chamber during reaction and thus endow it with enhanced catalytic activity for glucose hydrogenation compared to Ru−B/mSiO$_2$.

Figure 9 shows the reaction profile during one-pot dextrin conversion to sorbitol using the catalyst system containing both

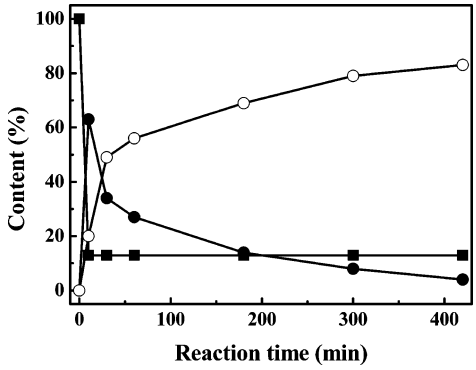

Figure 9. Reaction profile in one-pot hydrolysis-hydrogenation of dextrin by amyloglucosidase and Ru−B/mSiO$_2$@air@SiO$_2$. (■) dextrin, (●) glucose, and (○) sorbitol. Reaction conditions: dextrin (1.0 g), amyloglucosidase (0.08 mL), Ru−B/mSiO$_2$@air@SiO$_2$ (26 mg Ru), water (100 mL), T = 348 K, P_{H2} = 6.0 MPa, stirring rate = 800 rpm.

the free amyloglucosidase dissolved in aqueous solution and the Ru−B/mSiO$_2$@air@SiO$_2$. As shown in Figure 9, the amyloglucosidase catalyzed dextrin hydrolysis to glucose rapidly in the bulk solution, and nearly 87% of dextrin was converted within 10 min. Subsequently, the liberated glucose via dextrin hydrolysis diffused into the chamber by passing through the porous SiO$_2$ outer shell of Ru−B/mSiO$_2$@air@SiO$_2$, followed by hydrogenation to the final product, sorbitol, over the Ru−B amorphous alloy catalyst deposited onto the mesoporous SiO$_2$ support. The glucose hydrogenation proceeded smoothly, and sorbitol yield reached up to 83% after reaction for 7 h. Obviously, the porous SiO$_2$ outer shell preventing the diffusion of amyloglucosidase, dextrin, and colloidal substances resulted from dextrin hydrolysis into the chamber of the Ru−B/mSiO$_2$@air@SiO$_2$, which protected both the amyloglucosidase and the Ru−B catalysts from poisoning (Scheme 3). Meanwhile, such permeation-selective SiO$_2$ shells allowed the diffusion of reactant molecules due to their small molecular sizes, which could increase the accessibility and enhance the efficiency of glucose hydrogenation. To further confirm the key role played by the porous SiO$_2$ outer shell, we determined the reaction efficiencies in the one-pot dextrin conversion to sorbitol in the presence of free amyloglucosidase and the HF-treated Ru−B/mSiO$_2$@air@SiO$_2$ with different HF amounts and etching times (see Figure S5). One could see that, by using 1.0 mL of 40% HF, the dextrin conversion remained almost constant, but both the glucose conversion and the sorbitol yield increased with the increase of etching time up to 5 min. This could be easily understood by considering the increase of pore number and the enlargement of pore size on the outer SiO$_2$ shell, which promoted the diffusion of glucose into the chamber

Scheme 3. Schematic Illustration of the Separation of the Incompatible Catalysts in Different Region of the Yolk-Shell Structured Configuration

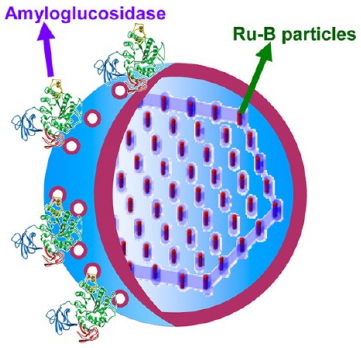

and the diffusion of the product sorbitol outside the chamber to the bulk solution, leading to the enhanced glucose hydrogenation rate. The dextrin conversion remained almost constant since the amyloglucosidase and the dextrin still could not diffuse into the chamber to contact the Ru−B. However, a further increase of the etching time to 7.5 min or an increase of the HF amount resulted in a decrease of dextrin conversion and glucose conversion, together with a decrease of sorbitol yield. A possible reason was that at a very high HF content or a very long etching time, some large-sized pores appeared on the outer SiO$_2$ shell. Thus, partial amyloglucosidase molecules might diffuse into the chamber to contact Ru−B located on the core, which poisoned each other, leading to the decrease of activity in both the dextrin hydrolysis and glucose hydrogenation. This was further confirmed by the fact that there was almost no conversion of either the dextrin or the glucose in one-pot dextrin conversion to sorbitol in the presence of mixed amyloglucosidase and crushed Ru−B/mSiO$_2$@air@SiO$_2$ obtained by grinding the original Ru−B/mSiO$_2$@air@SiO$_2$ (see Figure S6), implying the almost complete deactivation of the amyloglucosidase for dextrin hydrolysis and the Ru−B amorphous alloy catalyst for glucose hydrogenation to sorbitol.

Stability Studies. Besides the high efficiency, the Ru−B/mSiO$_2$@air@SiO$_2$ could be easily separated from the reaction solution *via* centrifugation and could be used repetitively eight times without a significant decrease in sorbitol yield in one-pot dextrin conversion to sorbitol using mixed amyloglucosidase and Ru−B/mSiO$_2$@air@SiO$_2$ as a catalyst system. As shown in Figure 10, at the end of the ninth cycle, the sorbitol yield decreased by 13%. By comparing the product distribution of the first run and the ninth run (Figure S7), it was found that the reused Ru−B/mSiO$_2$@air@SiO$_2$ (more than nine times) had no influence on the efficiency of amyloglucosidase for dextrin hydrolysis, but Ru−B/mSiO$_2$@air@SiO$_2$ partially lost its catalytic activity of glucose hydrogenation. ICP-OES analysis revealed that no leaching of Ru could be detected in the reaction mixtures during the repetitive runs, implying that this catalyst was stable against the chelating effect of the reactant and product. Meanwhile, the XRD pattern (Figure S8) demonstrated that the Ru−B in the Ru−B/mSiO$_2$@air@SiO$_2$ catalyst was still present in the amorphous alloy structure after being reused nine times, showing excellent stability against crystallization. The TEM image (Figure 11) showed that the Ru−B/mSiO$_2$@air@SiO$_2$ catalyst was still present in yolk-shell structure morphology and ordered mesoporous channels after

dx.doi.org/10.1021/cs400853u | ACS Catal. 2014, 4, 251−258

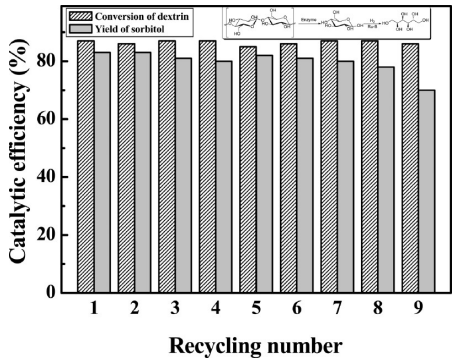

Figure 10. Recycling test of the combination of amyloglucosidase and Ru−B/mSiO$_2$@air@SiO$_2$ for one-pot hydrolysis−hydrogenation of dextrin. Reaction conditions are given in Figure 9. Each run was conducted for 7 h in recycling test.

being used repetitively nine times, implying high hydrothermal stability. However, the Ru−B nanoparticles partially aggregated, which might be the main factor responsible for the decrease in hydrogenation activity.

CONCLUSIONS

In summary, we developed a new approach to conducting one-pot cascade reactions for converting dextrin into sorbitol by using mixed amyloglucosidase and yolk-shell Ru−B/mSiO$_2$@air@SiO$_2$ as a catalyst system. In the Ru−B/mSiO$_2$@air@SiO$_2$, the porous outer SiO$_2$ shell encapsulated the Ru−B/mSiO$_2$ core comprising Ru−B amorphous alloy nanoparticles uniformly dispersed in ordered mesoporous channels of mSiO$_2$. Such a porous outer SiO$_2$ shell inhibited the diffusion of amyloglucosidase with a large molecular size into the chamber to contact Ru−B on the core, which avoided the poisoning effect on each other. Meanwhile, it also prevented the diffusion of dextrin with a big molecular size into the chamber but allowed the diffusion of glucose and product sorbitol inside the chamber owing to their small molecular sizes. As a result, the amyloglucosidase catalyzed the dextrin hydrolysis to glucose in bulk solution, followed by glucose hydrogenation to sorbitol on the Ru−B/mSiO$_2$ catalyst, leading to the high reaction efficiencies. This work might provide a general method for a one-pot cascade reaction with two kinds of catalysts which might poison each other.

ASSOCIATED CONTENT

Supporting Information

N$_2$ physisorption experiment of mSiO$_2$, low-angle XRD patterns of samples, effect of Ru loading on glucose hydrogenation and active surface areas of Ru−B/mSiO$_2$, characterization of the pure SiO$_2$ after being etched in HF solution, DSL determination of the size distribution of amyloglucosidase and amyloglucosidase/dextrin in aqueous solution, the effect of treating conditions on the dextrin conversion by enzyme and Ru−B/mSiO$_2$@air@SiO$_2$, FESEM image of the crushed Ru−B/mSiO$_2$@air@SiO$_2$, and recycle experiment results. This information is available free of charge via the Internet at http://pubs.acs.org/.

AUTHOR INFORMATION

Corresponding Author

*Tel.: +86-21-64322272. Fax: +86-21-64322272. E-mail: lihui@shnu.edu.cn.

Notes

The authors declare no competing financial interest.

ACKNOWLEDGMENTS

This work is supported by the National Natural Science Foundation of China (21273149), PCSIRT (IRT1269), the Program for New Century Excellent Talents in University (NCET-11-1052), and the Shanghai Science & Technology and Education Committee (11JC1408900, 12490502800, 10SG41, 12YZ084).

REFERENCES

(1) Werpy, T.; Peterson, G. *Top Value Added Chemicals from Biomass, Vol. 1: Results of Screening for Candidates from Sugars and Synthesis Gas.* U. S. Department of Energy, Energy Efficiency and Renewable Energy, Battelle: Richland, WA. http://www1.eere.energy.gov/biomass/pdfs/35523.pdf.

(2) Corma, A.; Iborra, S.; Velty, A. *Chem. Rev.* **2007**, *107*, 2411.

(3) Dhepe, P. L.; Fukuoka, F. *Catal. Surv. Asia* **2007**, *11*, 186.

(4) Fedor, W. S.; Millar, J.; Accola, A. J. *Ind. Eng. Chem.* **1960**, *52*, 282.

(5) Kruse, W. M.; Wright, L. W. *Carbohydr. Res.* **1978**, *64*, 293.

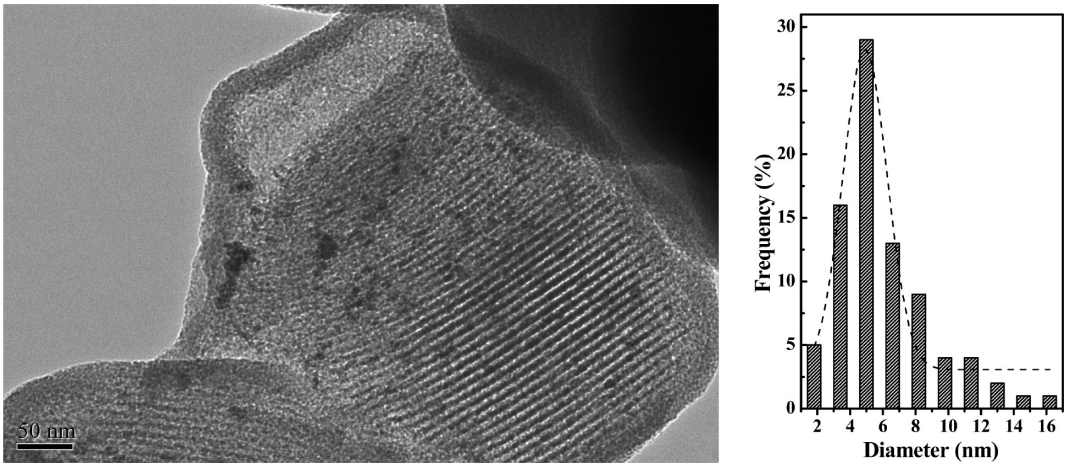

Figure 11. TEM image (left) and the corresponding Ru−B size distribution histogram (right) of the Ru−B/mSiO$_2$@air@SiO$_2$ catalyst after being reused nine times.

(6) Gallezot, P.; Cerino, P. J.; Blanc, B.; Fleche, G.; Fuertes, P. *J. Catal.* **1994**, *146*, 93.
(7) Kolaric, S.; Sunjic, V. *J. Mol. Catal. A* **1996**, *110*, 189.
(8) Li, H.; Li, H. X.; Deng, J. F. *Catal. Today* **2002**, *74*, 53.
(9) Guo, H. B.; Li, H. X.; Zhu, J.; Ye, W. H.; Qiao, M. H.; Dai, W. L. *J. Mol. Catal. A* **2003**, *200*, 213.
(10) Schimpf, S.; Louis, C.; Claus, P. *Appl. Catal., A* **2009**, *356*, 112.
(11) Sapunov, V. N.; Grigoryev, M. Ye.; Sulman, E. M.; Konyaeva, M. B.; Matveeva, V. G. *J. Phy. Chem. A* **2013**, *117*, 4073.
(12) Kadokawa, J. *Chem. Rev.* **2011**, *111*, 4308.
(13) Yankov, D.; Dobreva, E.; Beschkov, V.; Emanuilova, E. *Enzyme Microb. Technol.* **1986**, *8*, 665.
(14) Hoover, R. *Food Rev. Int.* **2000**, *16*, 369.
(15) Bruggink, A.; Schoevaart, R.; Kieboom, T. *Org. Process Res. Dev.* **2003**, *7*, 622.
(16) Climent, M. J.; Corma, A.; Iborra, S. *Chem. Rev.* **2011**, *111*, 1072.
(17) Simons, C.; Hanefeld, U.; Arends, I. W. C. E.; Maschmeyer, T.; Scheldon, R. A. *Top. Catal.* **2006**, *40*, 35.
(18) Heinen, A. W.; Papadogignakis, G.; Sheldon, R. A.; Peters, J. A.; van Bekkum, H. *J. Mol. Catal. A* **1999**, *142*, 17.
(19) Jacobs, P.; Hinnekens, H. EP 329923, 1988.
(20) Othmer, K. *Kirk-Othmer Encyclopedia of Chemical Technology*; 5th ed.; Wiley Interscience: New York, 2005; Vol. *10*, pp 248−317.
(21) Santiso, E. E.; George, A. M.; Heath Turner, C.; Kostov, M. K.; Gubbins, K. E.; Buongiorno-Nardelli, M.; Sliwinska-Bartkowiak, M. *Appl. Surf. Sci.* **2005**, *252*, 766.
(22) Pan, X.; Fan, Z.; Chen, W.; Ding, Y.; Luo, H.; Bao, X. *Nat. Mater.* **2007**, *6*, 507.
(23) Wang, Y.; Xu, L.; Xu, L.; Li, H. X.; Li, H. *Chin. J. Catal.* **2013**, *34*, 1027.
(24) Chen, S. Y.; Jang, L. Y.; Cheng, S. *Chem. Mater.* **2004**, *16*, 4174.
(25) Chen, D.; Li, L.; Tang, F.; Qi, S. *Adv. Mater.* **2009**, *21*, 3804.
(26) Scholten, J. J. F.; Pijers, A. P.; Hustings, A. M. L. *Catal. Rev.: Sci. Eng.* **1985**, *27*, 151.
(27) Li, H.; Li, H. X.; Dai, W. L.; Wang, W. J.; Fang, Z. G.; Deng, J. F. *Appl. Surf. Sci.* **1999**, *152*, 25.
(28) Klein, S.; Martens, J. A.; Parton, R.; Vercruysse, K.; Jacobs, P. A.; Maier, W. F. *Catal. Lett.* **1996**, *38*, 209.
(29) Li, H.; Zhu, Z. H.; Zhang, F.; Xie, S. H.; Li, H. X.; Li, P.; Zhou, X. G. *ACS Catal.* **2011**, *1*, 1604.